frontiers | Frontiers in Marine Science

TYPE Original Research
PUBLISHED 23 September 2022
DOI 10.3389/fmars.2022.999151

OPEN ACCESS

EDITED BY
Wei Cheng,
Center, Taipei, Taiwan

REVIEWED BY
Arthur Ayres Neto,
Fluminense Federal University, Brazil
Mauro Agate,
University of Palermo, Italy

*CORRESPONDENCE
Cunyong Zhang
ouczhangcunyong@163.com

SPECIALTY SECTION
This article was submitted to Coastal Ocean Processes, a section of the journal Frontiers in Marine Science

RECEIVED 20 July 2022
ACCEPTED 05 September 2022
PUBLISHED 23 September 2022

CITATION
Zhang C and Hou J (2022) Creep characteristics of muddy submarine channel slope instability. *Front. Mar. Sci.* 9:999151. doi: 10.3389/fmars.2022.999151

Creep characteristics of muddy submarine channel slope instability

Cunyong Zhang* and Jiankang Hou

School of Marine Technology and Geomatics, Jiangsu Ocean University, Lianyungang, China

Creep is an important factor of muddy submarine channel slope instability. In this study, a sub-bottom profiler was used to monitor the continuous internal change of a muddy submarine channel slope in the laboratory to better understand the creep characteristics and mechanism of slope instability. The creep process was analyzed according to changes in the slope internal sound intensity. The results indicate a notable change of the creep characteristics during the slope instability process. Changes in the sound intensity time series decrease with increasing slope depth, and the fluctuation depth of the vertical sound intensity series varies during the slope creep process. The creep process of slope instability can be roughly divided into four stages based on the sub-bottom profile data: an expansion stage; an unstable expansion stage; a fracture stage; and a post-fracture development stage. An adjustment of the sediment microstructure in the slope is ascribed to slope creep deformation. This study highlights the prospects of high-resolution acoustic monitoring to detect and quantify the entire creep process of muddy submarine channel slope instability, which is of great significance for the evaluation and early warning prediction of channel slope instability.

KEYWORDS

muddy submarine channel, slope, instability, creep, sub-bottom profiler

1 Introduction

Understanding muddy submarine channel slope creep behavior is of great importance owing to its close relation to slope collapse (Chang et al., 2020). Creep is a gradual slow deformation, irrespective of the cause or nature of this deformation (Baba et al., 2015). The sea water particularly acts on the submarine channel slope in the form of waves, flow, and tides (Georg, 1974). Once creep accumulates to a certain extent, triggered by natural phenomena (e.g., storm surges) and human activities (e.g., ship traffic) (Sultan et al., 2004), the channel slope may destabilize, which can change the channel geometry, block ports, and cause marine traffic accidents.

The creep of muddy submarine channel slope instability is a transient process that has a time-dependent behavior (Leynaud et al., 2009; Chang et al., 2015). The recognition of the internal creep process of channel slopes and analysis of its deformation mechanism is therefore useful to predict their instability. However, channel slope creep is difficult to investigate using fixed-point measurements owing to seawater turbidity and challenges involved in approaching the seabed. Conventional methods, such as laboratory creep tests using drilling samples (Dai and Santamarina, 2014), are impractical for interpreting and describing the internal creep process of channel slopes owing to limited samples. It is also challenging to quantify the internal creep evolution of a slope using traditional methods, such as triaxial creep tests (Tran et al., 2018).

Sub-bottom profiling is a type of seabed acoustic mapping technology that uses the propagation and reflection characteristics of acoustic waves in seawater and seabed sediments to continuously detect seabed sediments and obtain visual sub-bottom profiles (He et al., 2022). The acoustic characteristics and internal organization of sediments have certain effects on the propagation of acoustic waves (Hamilton and Bachman, 1982). When a slope creeps, the internal sediment physical properties (e.g., structure, density) change, which accordingly affects the propagation velocity, energy attenuation, and spectral composition of the acoustic waves. These changes can be delineated by an acoustic profile image composed of dot, block, or linear patterns with certain sound intensities (Mosquera et al., 2014). Few studies have investigated the internal creep process and characteristics of muddy submarine channel slope instability, thus its creep behavior remains poorly understood. To address this problem, sub-bottom profile acoustic images were used to study the creep characteristics and muddy submarine channel slope instability process. The creep mechanism was analyzed to better understand the creep properties of muddy submarine channel slope instability.

2 Materials and methods

2.1 Creep observation

The complete submarine channel slope instability process is difficult to observe in the field, thus this process was simulated in a laboratory flume (Figure 1). The experiment was carried out in the seabed exploration laboratory of Jiangsu Ocean University. The width, length, and depth of the laboratory flume were 2 m, 4 m, and 2.5 m, respectively. The depth of water in the laboratory flume was 2.3 m. A channel slope model was built at a 45° slope with a height of 130 cm using sediment from the Lianyungang channel, which is a typical deep-water navigation channel located in a muddy shoal of an open bay on the western coast of the Yellow Sea. The sediments in the main channel are primarily composed of mud (Xie et al., 2010). The main mineral components of the sediments include clay minerals (19%-54%), quartz (28%-56%), plagioclase (11%-17%), potassium feldspar (2%-6%), and calcite (up to 2%) according to the total mineral analysis (Liu et al., 2011). The undisturbed shear strength, remolded shear strength, and sensitivity ranges are 10.9-34.8 kPa, 1.6-15.8 kPa, and 1.6-8.5, respectively (Wu et al., 2020).

The creep process was continuously measured using an SES-2000 acoustic parametric array sub-bottom profiler (Innomar Technologie GmbH, Rostock, Germany), which was installed in the laboratory flume aimed at a fixed shoulder section of the slope to obtain data covering the full channel slope instability process. The transducer was mounted to the tank track using a telescopic stand, which can be adjust the height to the slope. The transducer is 0.5m above the slope. Sub-bottom profiles were collected in single frequency mode. The low frequency was set to 15 kHz. The maximum ping rate was set to the system default. The pulse duration was set to 133 milliseconds (Zhang, 2021).

Currents simulated using a submersible pump were used as hydrodynamic forces. The current velocity was 0.5 m/s. The change of internal structure of the slope under the hydrodynamic force was continuously monitored by the monitor of the SES-2000 system until a complete channel slope instability process was captured. All original data were recorded on the system memory chip.

The sub-bottom profile images are the echograms from the echo data by post processing software of the SES-2000 system. For a sub-bottom profile image of m×n pixel size, it can be regarded as a m×n matrix. Each element in the matrix corresponds to the value of sound intensity for a particular point of the slope. The change of sound intensity usually reflects the change of internal structure of the slope. The vertical axis of the slope profile image indicates depth, and the horizontal axis indicates time in order to identify the changes in the internal structure of the slope.

This study focuses on the creep process from sub-bottom profile images. To analyze variations in sound intensity as functions of both time and space, the one-dimensional components of these matrices in the temporal and vertical spatial domains were extracted. To maintain focus on the creep process occurring in the sediments, the overlying water of the sediments was clipped using post-processing software included in the SES-2000 profiler system.

2.2 Microstructure observation

The samples before, during, and after channel slope instability were collected from the channel slope at different depths (slope top, middle part of the slope, and slope bottom) using a plastic tube. The samples collected before, during, and after slope instability were from the same level. The samples

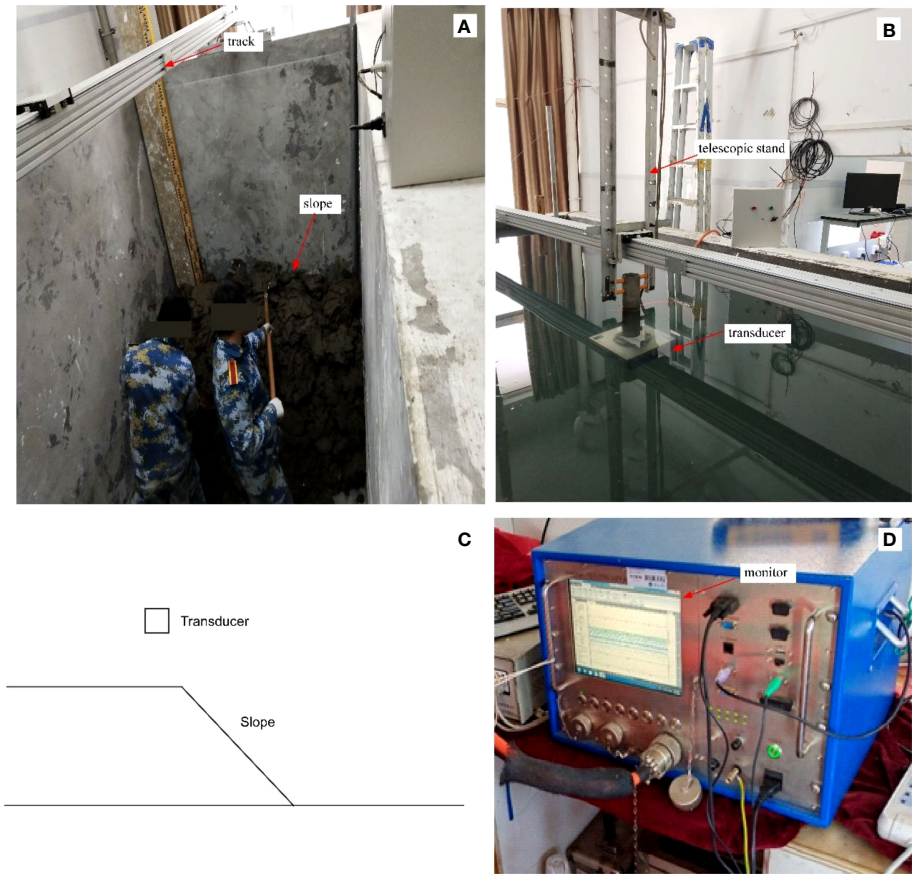

FIGURE 1
Experimental set-up **(A)** slope, **(B)** transducer, **(C)** slope schematic diagram, **(D)** monitor (Zhang, 2022).

collected from the slope at different depths were at the same stage (after slope instability). Then, the samples were extracted and allowed to dried naturally. After obtaining a fresh surface by breaking, the samples were cut into approximately 6 × 6 mm blocks using a sharp thin knife. The sample microstructure was investigated by scanning electron microscope (SEM, JSM-6390LA type, JEOL Company, Japan) at the SEM laboratory of Jiangsu Ocean University. The SEM observation process was as follows.

1. Conductive adhesive of an appropriate size was pasted on the sample holder and prepared samples contained within it.
2. The samples were placed into a vacuum ion sputtering instrument and a thin layer of gold film was deposited.
3. The samples were placed in the sample chamber of the SEM for scanning from low to high magnification.
4. After adjusting the focal length and contrast, SEM images of 500, 1000, 2000, 3000, and 10,000 times magnification were compared to ensure that the acquired image portrayed the target information. At lower magnification, the image was insufficiently clear for particle analysis, whereas at higher magnification, the image reflected more localized features but not overall features (Zhou et al., 2021).
5. After comparison, the image with 1000 times magnification was selected for microstructural investigation.

3 Results

3.1 Creep deformation characteristics of channel slope instability

The creep characteristics acquired from the sub-bottom profile images provide abundant internal texture details of the slope. In the sub-bottom profile images, the creep process is displayed as a distinct and irregular texture with alternating

strong and weak intensities. Figure 2 shows a typical diagram of the creep process, where high and low intensities are represented by yellow and blue color, respectively. The creep characteristics exhibit gradual and continuous but recognizable changes. In the initial expansion stage of creep, the creep texture features begin to deform from parallel stripes to irregularities, roughness, and fractures expressed in the width and intensity of the near-parallel stripes. Creep deformation mainly occurs in the upper part of the slope and gradually expands to the slope interior (Figure 2A). As the process develops, the creep texture extends forward in an approximately parallel state, appears increasingly fluffy, bifurcated, and fractured, continues to roughen, and the strength becomes increasingly large and uneven (Figure 2B). The extension length of the upper creep texture is larger than that of the lower creep textures. With increasing creep time, the creep texture appears increasingly wavy and the strength increases (Figure 2C). Different creep textures become crossed, separated, and merge, and the intensity increases (Figure 2D). As time proceeds, the creep textures at the upper part of the slope become discontinuous and fluctuate with intermittent intensity changes. The creep textures appear deformed in the lower part of the slope (Figure 2E). When the creep accumulates to a certain extent, the creep texture features show notable sliding fractures, bending fractures, and staggered breakage (Figure 2F). These features demonstrate that the sub-bottom profile images visually exhibit the full stages of the creep process of channel slope instability, which are not perceptible using conventional laboratory creep experiments using limited samples.

3.2 Creep strength characteristics of channel slope instability

3.2.1 Sound intensity time series changes during creep

During the slope creep process, sub-bottom profile images are generated as a set of visual and continuous sound profile images comprising an ordered set of sound intensity pixels. Each pixel corresponds to the sound intensity value for a particular point of the slope. The creep evolution during slope instability can be quantitatively described by the sound intensity. Because the creep varies with depth from the top to bottom of the slope, the typical sound intensity time series of the top, middle, and bottom of the channel slope are selected to demonstrate the sound intensity variation during the creep process. Figure 3 illustrates the sound intensity time series variations during the full creep process of slope instability based on the sub-bottom profile images. The figures show that the sound intensity undergoes nonlinear changes, which decrease with increasing slope depth.

The creep process of slope instability can be roughly divided into four stages according to the sound intensity changes: an expansion stage; an unstable expansion stage; a fracture stage; and a post-fracture development stage. During the expansion stage, the change of the sound intensity is essentially stable with increasing time. The sound intensity amplitude is small, and the change curve is generally nearly horizontal and roughly parallel to the abscissa axis. During the unstable expansion stage, the sound intensity gradual increases from 6500 s through 15,280 s. The change of the sound intensity amplitude begins to gradually increase, indicating a rapid increase of creep deformation. In the fracture stage, an abrupt rise in sound intensity appears from 15,280 s through 15,380 s. However, the rapid rise of sound intensity terminates quickly (within ~100 s). The sound intensity rapidly increases and the maximum of sound intensity amplitude change occurs over a short time, which reflects the slope fracture. Following the fracture stage, the change of sound intensity decreases and the sound intensity amplitude remains relatively stable, which indicates the creep will continue into next cycle after failure. The nonlinear fluctuation of sound intensity time series during the creep process show that the slope becomes fractured after multiple cumulative creep episodes to a certain extent.

3.2.2 Vertical sequence change of sound intensity during creep

In addition to sound intensity changes with time during the channel slope creep process, the vertical sound intensity also exhibits substantial changes. Figure 4 shows the typical vertical sound intensity variation of the three different stages during the creep process of slope instability. The vertical sequence change of the sound intensity presents multiple peaks during the creep process, with an overall decreasing trend as well as fluctuations to different depths. As is shown in Figure 4, the vertical sound intensity changes have distinct oscillation characteristics (e.g., amplitude, frequency) at certain depths and in different stages. During the expansion stage (Figure 4A), the sound intensity change is relatively small and high-frequency oscillation changes mainly occur in the shallow part of slope. In the unstable expansion stage (Figure 4B), the sound intensity increases unevenly. In the fracture stage (Figure 4C), the sound intensity continually increases and the oscillation peaks extend to the deeper part of the slope. In the post-fracture development stage (Figure 4D), the change of sound intensity becomes smaller and the oscillation depth becomes shallow. As the slope creep proceeds, the abscissa of the peak vertical sound intensity value exhibit notable changes with depth.

3.3 Microstructure changes of the channel slope

Microstructure typically refers to the size, shape, arrangement, contact, and connection of particles and the overall porosity (Xie et al., 2018). The SEM observations of the sample microstructures before, during, and after slope instability

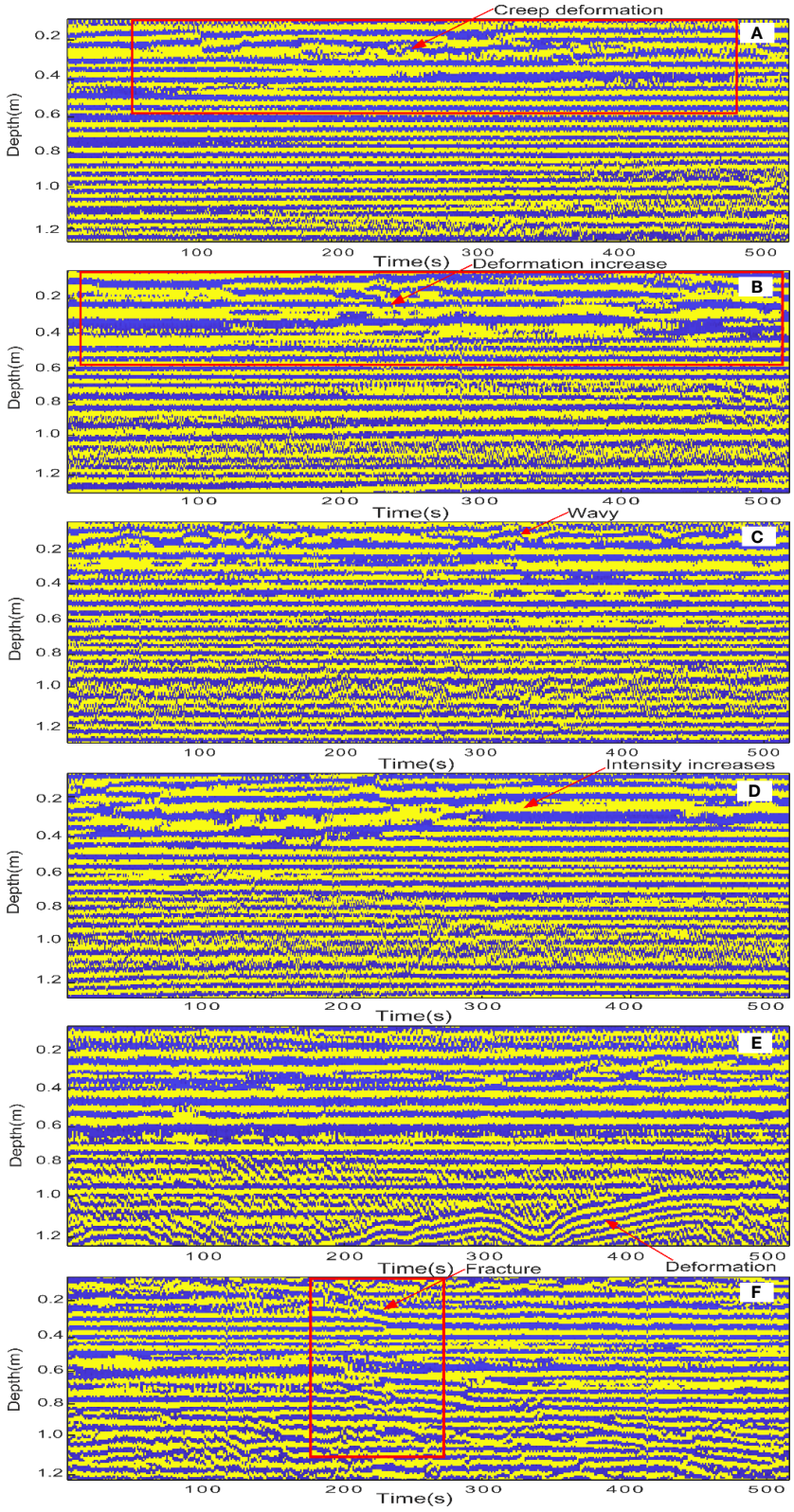

FIGURE 2
Typical deformation characteristics of slope instability obtained from sub-bottom profile images. **(A-F)** indicate different deformation state.

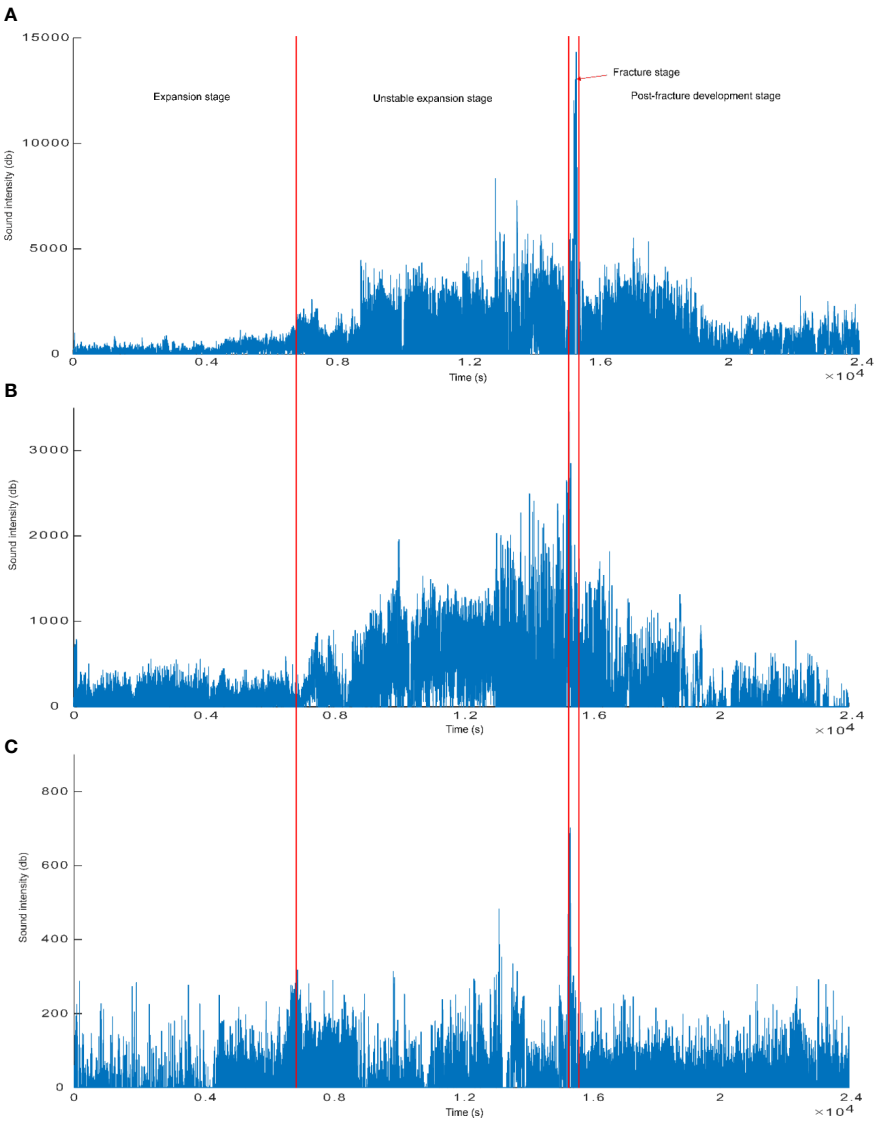

FIGURE 3
Typical sound intensity time series variation during the creep process of the **(A)** surface, **(B)** middle, and **(C)** bottom layer of the slope.

are shown in Figure 5. The size, shape, and adhesion between the aggregates and particles is found to substantially change with slope instability. Prior to creep, the samples possessed aggregates and particles of different shapes and sizes (granular and angular). The interaggregate or particle pores are observed (Figure 5A). During creep, the aggregates and particles are compacted into a denser structure (Figure 5B). Many larger aggregates disappear. After creep, the samples show a preferred parallel flocculated structure (Figure 5C). Those elongated flocs and particles are looser and relatively uniform with significant orientation. Pore enlargement is caused by the reorientation and movement of floc and particles. The microstructure changes during the creep process of slope instability are therefore manifested not only by changes of the interaggregate pores, but also the reorientation and rearrangement of flocs and particles.

The SEM images also show that the microstructure varies from the top to bottom of the slope. On the slope top, the sample has high porosity, is relatively loose, and large-sized interaggregate pores with various sizes of small pores are distinct (Figure 5D). In the middle part of the slope, the large-sized interaggregate pores disappear and the distribution of aggregates and particles is more intensive (Figure 5E). On the slope bottom, the flocculated structure is well developed and a dense arrangement of smaller flocs and particles is distinct (Figure 5F). With increasing depth, the change of the interaggregate pores becomes dominant and the microstructure becomes denser.

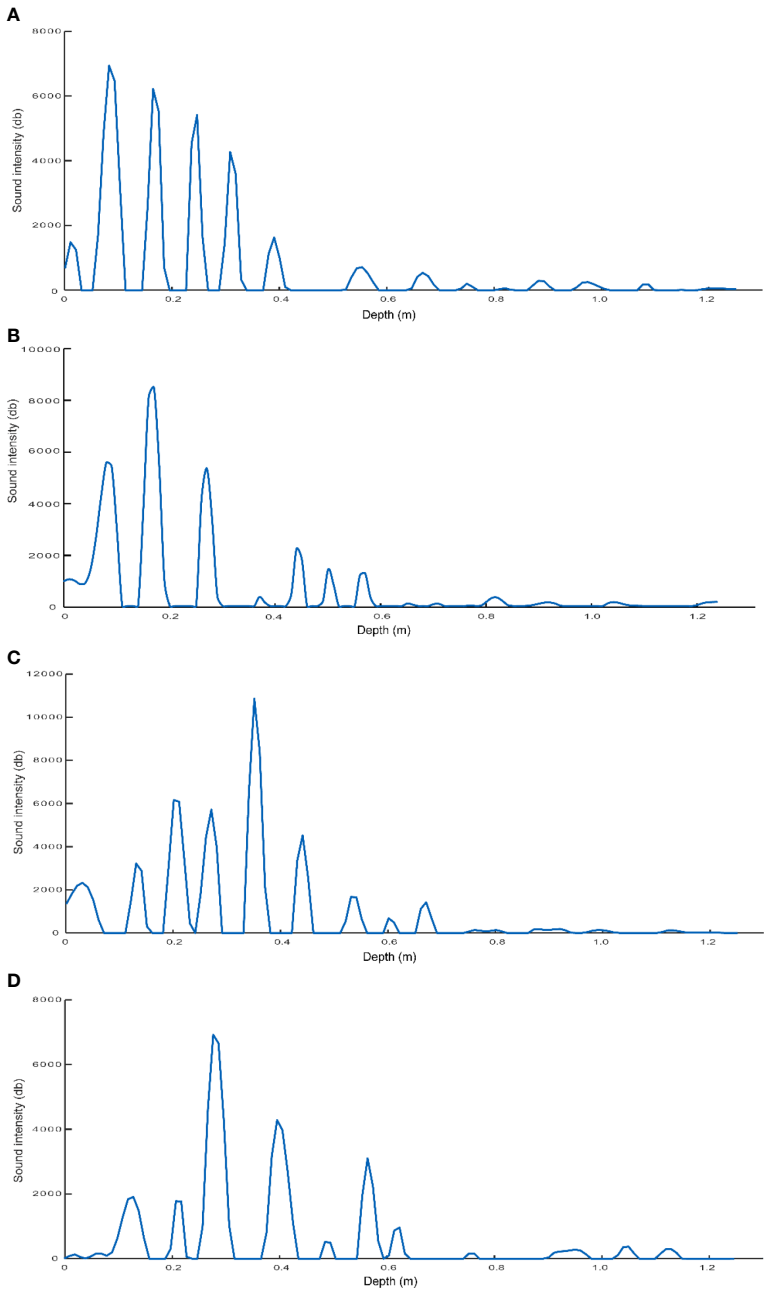

FIGURE 4
Vertical sequence change of the sound intensity during different creep stages: **(A)** expansion stage; **(B)** unstable expansion stage; **(C)** fracture stage; **(D)** post-fracture development stage.

4 Discussion

4.1 Creep mechanism of channel slope instability

Several studies have shown that effective macro characteristics are an external embodiment of the microstructure, and that the macro characteristics of slope creep are affected by microstructural changes (Sun et al., 2020; Zheng et al., 2021). Muddy submarine channel slope soil is a kind of structurally soft soil, which has characteristic properties of high water content, low strength, remarkable structure deformation and longer duration (Wang et al., 2014; Wu et al., 2021). Under the action of periodic cyclic loading, a series of

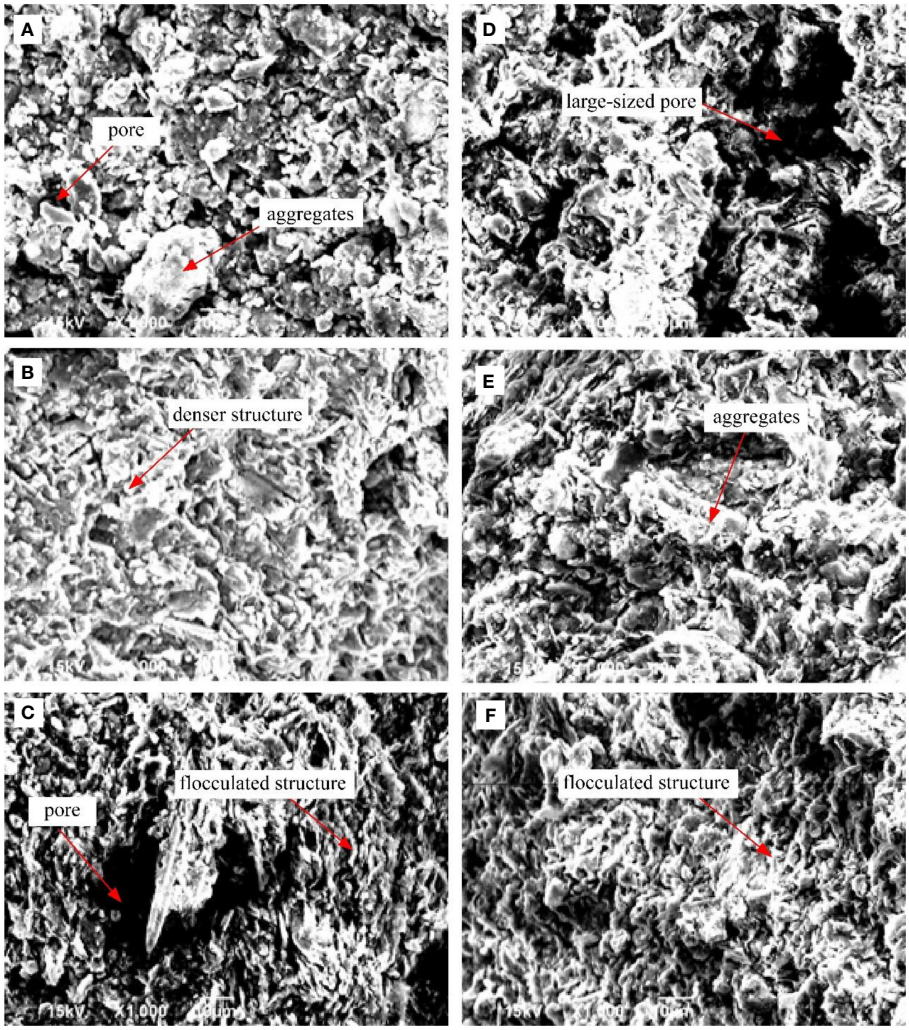

FIGURE 5
SEM images of samples **(A)** before, **(B)** during, and **(C)** after channel slope instability, and **(D)** top, **(E)** middle, and **(F)** bottom part of the slope.

dynamic response processes will occur in the slope sediments and the stress will concentrate in some parts. The weakest part of the structure begins to change, resulting in relative displacement and particle rearrangement. Under the action of rotation, slipping, and squeezing, the aggregates or particles are broken into smaller aggregates or particles, and the aggregates with weak connection forces between the particles are condensed into new aggregates. The connecting force between particles can thus balance the external force. When the soil particles of the slope are rearranged, the spatial position of the internal particles is adjusted and a new skeleton structure forms through the mutual extrusion combination among particles. Part of the water between the pores is discharged and the soil is deformed. As a result, the particle contacts increase and the skeleton particles change from point contacts to aggregate overlapping contacts, thus enhancing the mutual restraint. As creep continues, the internal structure of the soil begins to be destroyed, and the soil deformation accelerates until the slope destabilizes. Figure 5 illustrates the microstructure changes before, during, and after slope creep. Flocculated structures with skeletons consisting of aggregates and particles are exhibited before creep, whereas the microstructure shows a preferred parallel flocculated structure with large-sized interaggregate pores after slope creep.

Slope instability is affected by many factors (Baba et al., 2015). In general, shear strength and pore water pressure changes are the principal factors that govern slope instability (Sultan et al., 2004), which are primarily attributed to the microstructure and porous structure changes of soil during the slope creep process. As can be seen from Figure 4, the vertical sound intensity variation has distinct oscillation at certain depths. The inhomogeneous variation constantly increases and decreases along the depth, which represent the unevenly

mobilization of shear strength. Hydrodynamic forces weaken the soil shear strength and increase the pore water pressure by changing the microstructure, and the increasing pore water pressure reduces the effective stress (Lian et al., 2020). These are important factors that affect the stability of muddy submarine channel slopes.

4.2 Creep stages of channel slope instability

Both geological and rheological premises can be used to verify that slope instability is not a sudden phenomenon, but involves multi-temporal creep and requires a period of time to completely collapse (Georg, 1974). The creep process has traditionally been divided into three stages: primary creep; secondary creep; and tertiary creep (Tran et al., 2018). According to the classic interpretation, primary creep is the initial stage, secondary creep is the constant creep stage, and tertiary creep is the acceleration stage that leads to rupturing (Intrieri et al., 2019).

Figure 3 shows that the creep behavior of the muddy submarine channel slope mainly underwent a steady expansion stage, unstable expansion stage, fracture stage, and post-fracture development stage. The sound intensity varies greatly from the initial expansion stage to post-fracture development stage. The creep process of the middle part of slope is similar to that of the slope top, and resembles that of the slope bottom except for the amplitude. The creep thus undergoes a nonlinear process and cannot be described by a simple functional relationship. Various creep models proposed in previous studies (e.g., empirical models, component models, fractional viscoelastic models, creep damage models) (Gao and Yin, 2021) therefore do not accurately describe the slope internal creep. The visually and quantitatively sub-bottom profile method may be a useful alternative to understand the creep process.

4.3 Creep depth of channel slope instability

Creep depth can be an important reference for muddy submarine channel slope instability. The previously mentioned creep characteristics acquired from sub-bottom profile images indicate that creep mainly occurs in the upper part of the slope and gradually expands to the slope interior. Figure 4 show that the sound intensity peaks oscillate with depth from 0 m to 0.6 m. The deformation results (Figure 2) demonstrate that the fluctuating range corresponded well with the instability zone. The maximum peak depth may reflect the position of the potential sliding surface. Yan et al. (2017) confirmed the potential sliding surface in an experimental study based on Brillouin optical time-domain analysis.

Hydrodynamic forces reduce the effective stress of the slope by the periodic and cyclic loading of currents, waves, and tides. The inhomogeneous distribution of stress periodically increases and decreases in the vertical direction, which results in the formation of slope shear stress. The slope shear strength is unevenly mobilized depending on the cyclic load and geological conditions. The vertical sound intensity variation has distinct oscillation characteristics along the depth in Figure 4 represent the unevenly mobilization of shear strength. Creep aggravation enhances the shear strength mobilization, and the stress expands over the entire potential sliding surface. Creep depths that are closer to the potential sliding surface have a higher possibility of slope instability. This exemplifies why investigation should be pay a great attention on internal slope changes.

4.4 Creep detection of channel slope instability

All slow deformation is generally defined as creep, irrespective of the cause or nature of this deformation (Baba et al., 2015). Creep is a common phenomenon on submarine slopes (Sultan et al., 2004), but creep processes have rarely been reported on submarine slopes (Hill et al., 1982). This may be mainly related to a lack of technology to recognize the process. Traditional methods, such as borehole test (Sun et al., 2017), creep-meter (Wang et al., 2020), extensometer (Suwa et al., 2010), usually disturb slope creep by inserting a detection instrument, which seriously limits the reliability of the results (Brian, 1981). In addition, it is difficulty to investigate the internal creep process of channel slope completely using limited survey point. Those methods also usually represent one-dimensional creep, which does not provide internal two-dimensional details of the channel slope creep in space and time. However, a sub-bottom profiler can be used to obtain non-invasive, two-dimensional profile images with high resolution, which provide valuable information regarding the desired internal creep process and increases the data availability.

Visual interpretation is presently widely used to study deep-seated gravitational slope deformation (Carpentier et al., 2012). Moreover, shallow seismic method (Kühn et al., 2021), multichannel seismic method (Shillington et al., 2012), particle image velocimetry (Baba and Peth, 2012), ground penetrating radar (Gopaiah et al., 2021), and electrical resistivity tomography (Hojat et al., 2019) are proven methods that deliver the desired images. In contrast to other geophysical techniques, a sub-bottom profiler is more suitable for detecting muddy submarine channel slope creep process owing to its high resolution (Sitkiewicz et al., 2020), and its profile image is similar to a geological section map, which is convenient to interpret the internal creep process of channel slopes. To the best of our knowledge, a sub-bottom profiler has not been

previously reported in the literature to investigate the creep evolution process. This study demonstrates that sub-bottom profile images can quantitatively reflect the slope creep process by internal sound intensity variations, which provides a new approach for detecting the creep of muddy submarine channel slopes.

5 Conclusions

(1) A sub-bottom profiler was introduced to analyze the creep process of muddy submarine channel slope instability in the laboratory. The visual interpretation demonstrates that creep mainly occurs in the upper part of the slope and gradually expands to the slope interior. As creep develops, creep stress textures form at the bottom of the slope and texture fractures appear. The sub-bottom profile images visually present the internal creep process of muddy submarine channel slope instability using non-invasive acoustic monitoring technology.

(2) The sound intensity time series and vertical series present nonlinear characteristics which cannot be described by a simple functional relationship during the slope creep process. According to the sound intensity changes in the internal channel slope, the creep process of slope instability can be roughly divided into four stages instead of the classic interpretation. The sound intensity variations demonstrate that creep mainly occurs at the upper slope, and gradually expands to the slope interior. The vertical sound intensity variation has multiple peaks and distinct oscillation characteristics along the depth represent the unevenly mobilization of shear strength. The depth of the sound intensity changes varies during the different creep stages, which indicates that creep undergoes multiple accumulation processes.

(3) The macroscopic properties of slope creep are significantly affected by the sediment microstructure, which adapts to changes of the external forces by continuous self-adjustment, rearrangement and reconstruction of the internal sediment structure. The internal change of the channel slope is intuitively and quantitatively connected with the creep characteristics, which provides a basis for understanding the creep mechanism of muddy submarine channel slope instability.

Data availability statement

The raw data supporting the conclusions of this article will be made available by the authors, without undue reservation.

Author contributions

CZ analyzed data and wrote the paper. JH investigated the sample microstructure. Both authors contributed to the article and approved the submitted version.

Funding

This work was supported by the Key Research and Development Program of Jiangsu Province (grant number BE2018676), and the Graduate Research and Practice Innovation Program of Jiangsu Ocean University (grant number KYCX2021-026).

Acknowledgments

The authors would like to thank Wang X, Xu J, Wang Y, Feng J W, Liu Z Y, Liu T P, Li T Y, and Chang T Y, for their help with the fieldwork and laboratory experiments.

Conflict of interest

The authors declare that the research was conducted in the absence of any commercial or financial relationships that could be construed as a potential conflict of interest.

Publisher's note

References

Baba, H. O., and Peth, S. (2012). Large Scale soil box test to investigate soil deformation and creep movement on slopes by particle image velocimetry (PIV). *Soil Tillage Res.* 125, 38–43. doi: 10.1016/j.still.2012.05.021

Baba, H. O., Peth, S., Horn, R., Bens, O., and Hüttl, R. F. (2015). Quantification of mechanical strength and sliding stability of an artificial water catchment (Chicken creek). *Soil Tillage Res.* 146, 66–78. doi: 10.1016/j.still.2014.05.013

Brian, F. (1981). Field measurements of soil creep. *Earth Surf. Process. Landforms* 6, 35–48. doi: 10.1002/esp.3290060105

Carpentier, S., Konz, M., Fischer, R., Anagnostopoulos, G., Meusburger, K., and Schoeck, K. (2012). Geophysical imaging of shallow subsurface topography and its implication for shallow landslide susceptibility in the urseren valley, Switzerland. *J. Appl. Geophys.* 83, 46–56. doi: 10.1016/j.jappgeo.2012.05.001

Chang, Z., Gao, H., Huang, F., Chen, J., Huang, J., and Guo, Z. (2020). Study on the creep behaviours and the improved burgers model of a loess landslide considering matric suction. *Natural Hazards* 103, 1479–1497. doi: 10.1007/s11069-020-04046-0

Chang, K. T., Ge, L., and Lin, H. H. (2015). Slope creep behavior: observations and simulations. *Environ. Earth Sci.* 73, 275–287. doi: 10.1007/s12665-014-3423-2

Dai, S., and Santamarina, J. C. (2014). Sampling disturbance in hydrate-bearing sediment pressure cores: NGHP-01 expedition, Krishna-godavari basin example. *Mar. Pet. Geol.* 58, 178–186. doi: 10.1016/j.marpetgeo.2014.07.013

Gao, Y., and Yin, D. (2021). A full-stage creep model for rocks based on the variable-order fractional calculus. *Appl. Math. Model.* 95, 435–446. doi: 10.1016/j.apm.2021.02.020

Georg, T. S (1974). Depth creep of slopes. *Bulletin of the International Association of Engineering Geology* 9, 97–102. doi: 10.1007/BF02635311

Gopaiah, M., Saha, R., Chandra, D. I., Sankar, G. J., and Kumar, K. V. (2021). Quantitative assessment of aquifer potential in near shore coastal region using geospatial techniques and ground penetrating radar. *Estuarine Coast. Shelf Sci.* 262, 107590. doi: 10.1016/j.ecss.2021.107590

Hamilton, E. L., and Bachman, R. T. (1982). Sound velocity and related properties of marine sediments. *J. Acoust. Soc. America* 72 (6), 1891–1904. doi: 10.1121/1.388539

He, L., Zhao, J., Lu, J., and Qiu, Z. (2022). High-accuracy acoustic sediment classification using sub-bottom profile data. *Estuarine Coast. Shelf Sci.* 265, 107701. doi: 10.1016/j.ecss.2021.107701

Hill, P. R., Moran, K. M., and Blasco, S. M. (1982). Creep deformation of slope sediments in the Canadian Beaufort Sea. *Geo-Marine Lett.* 2, 163–170. doi: 10.1007/BF02462758

Hojat, A., Arosio, D., Ivanov, V. I., Longoni, L., Papini, M., Scaioni, M., et al. (2019). Geoelectrical characterization and monitoring of slopes on a rainfall-triggered landslide simulator. *J. Appl. Geophys.* 170, 103844. doi: 10.1016/j.jappgeo.2019.103844

Intrieri, E., Carlà, T., and Gigli, G. (2019). Forecasting the time of failure of landslides at slope-scale: A literature review. *Earth-Sci. Rev.* 193, 333–349. doi: 10.1016/j.earscirev.2019.03.019

Kühn, M., Karstens, J., Berndt, C., and Watt, S. F. L. (2021). Seismic reconstruction of seafloor sediment deformation during volcanic debris avalanche emplacement offshore sakar, Papua new Guinea. *Mar. Geol.* 439, 106563. doi: 10.1016/j.margeo.2021.106563

Leynaud, D., Mienert, J., and Vanneste, M. (2009). Submarine mass movements on glaciated and non-glaciated European continental margins: A review of triggering mechanisms and preconditions to failure. *Mar. Pet. Geol.* 26, 618–632. doi: 10.1016/j.marpetgeo.2008.02.008

Lian, B., Peng, J., Zhan, H., Huang, Q., Wang, X., and Hu, S. (2020). Formation mechanism analysis of irrigation-induced retrogressive loess landslides. *Catena* 195, 104441. doi: 10.1016/j.catena.2019.104441

Liu, S. Y., Shao, G. H., Du, Y. J., and Cai, G. J. (2011). Depositional and geotechnical properties of marine clays in lianyungang, China. *Eng. Geol.* 121, 66–74. doi: 10.1016/j.enggeo.2011.04.014

Mosquera, R., Groposo, V., and Pedocchi, F. (2014). Acoustic measurements of a liquefied cohesive sediment bed under waves. *Adv. Geosci.* 39 (39), 1–7. doi: 10.5194/adgeo-39-1-2014

Shillington, D. J., Seeber, L., Sorlien, C. C., Steckler, M. S., Kurt, H., Dondurur, D., et al. (2012). Evidence for widespread creep on the flanks of the Sea of marmara transform basin from marine geophysical data. *Geology* 40 (5), 439–442. doi: 10.1130/G32652.1

Sitkiewicz, P., Rudowski, S., Wróblewski, R., and Dworniczak, J. (2020). New insights into the nearshore bar internal structure using high-resolution sub-bottom profiling: The vistula spit case study. *Mar. Geol.* 419, 106078. doi: 10.1016/j.margeo.2019.106078

Sultan, N., Cochonat, P., Canals, M., Cattaneo, A., Dennielou, B., Haflidason, H., et al. (2004). Triggering mechanisms of slope instability processes and sediment failures on continental margins: a geotechnical approach. *Mar. Geol.* 213, 291–321. doi: 10.1016/j.margeo.2004.10.011

Sun, H., Hou, M., Chen, C., and Ge, X. (2020). Microstructure investigation of soft clay subjected to triaxial loading. *Eng. Geol.* 274, 105735. doi: 10.1016/j.enggeo.2020.105735

Sun, Z., Wang, Y., Sun, Y., Niu, F., Li, G., and Gao, Z. (2017). Creep characteristics and process analyses of a thaw slump in the permafrost region of the qinghai-Tibet plateau, China. *Geomorphology* 293, 1–10. doi: 10.1016/j.geomorph.2017.04.045

Suwa, H., Mizuno, T., and Ishii, T. (2010). Prediction of a landslide and analysis of slide motion with reference to the 2004 ohto slide in Nara, Japan. *Geomorphology* 124, 157–163. doi: 10.1016/j.geomorph.2010.05.003

Tran, T. T. T., Hazarika, H., Indrawan, I. G. B., and Karnawati, D. (2018). Prediction of time to soil failure based on creep strength reduction approach. *Geotech. Geol. Eng.* 36, 2749–2760. doi: 10.1007/s10706-018-0496-9

Wang, J., Guo, C., Hou, Z., Fu, Y., and Yan, J. (2014). Distributions and vertical variation patterns of sound speed of surface sediments in south China Sea. *J. Asian Earth Sci.* 89, 46–53. doi: 10.1016/j.jseaes.2014.03.026

Wang, X., Wang, J., Zhan, H., Li, P., Qiu, H., and Hu, S. (2020). Moisture content effect on the creep behavior of loess for the catastrophic baqiao landslide. *Catena* 187, 104371. doi: 10.1016/j.catena.2019.104371

Wu, Z., Deng, Y., Cui, Y., Chu, C., and Qi, F. (2020). Geological investigation of the settlement behaviour of two highways in lianyungang region. *Eng. Geol.* 272, 105648. doi: 10.1016/j.enggeo.2020.105648

Wu, J., Xuan, Y., Deng, Y., Li, X., Zha, F., and Zhou, A. (2021). Combined vacuum and surcharge preloading method to improve lianyungang soft marine clay for embankment widening project: A case. *Geotextiles Geomembranes* 49, 452–465. doi: 10.1016/j.geotexmem.2020.10.013

Xie, X., Qi, S., Zhao, F., and Wang, D. (2018). Creep behavior and the microstructural evolution of loess-like soil from xi'an area, China. *Eng. Geol.* 236, 43–59. doi: 10.1016/j.enggeo.2017.11.003

Xie, M. X., Zhang, W., and Guo, W. J. A. (2010). Validation concept for cohesive sediment transport model and application on lianyungang harbor, China. *Coast. Eng.* 57 (6), 585–596. doi: 10.1016/j.coastaleng.2010.01.003

Yan, J. F., Shi, B., Ansari, F., Zhu, H. H., Song, Z. P., and Nazarian, E. (2017). Analysis of the strain process of soil slope model during infiltration using BOTDA. *Bull. Eng. Geol. Environ.* 76, 947–959. doi: 10.1007/s10064-016-0916-0

Zhang, C. (2021). Slope instability detection for muddy submarine channels using sub-bottom profile images based on bidimensional empirical mode decomposition. *Geo-Marine Lett.* 41, 1. doi: 10.1007/s00367-020-00681-5

Zhang, C. (2022). Fractal analysis of muddy submarine channel slope instability from sub-bottom profile images. *Mar. Georesour. Geotechnol.* 40 (6), 701–711. doi: 10.1080/1064119X.2021.1933278

Zheng, Y., Sun, H., Hou, M., and Ge, X. (2021). Microstructure evolution of soft clay under consolidation loading. *Eng. Geol.* 293, 106284. doi: 10.1016/j.enggeo.2021.106284

Zhou, C., Yu, L., Huang, Z., Liu, Z., and Zhang, L. (2021). Analysis of microstructure and spatially dependent permeability of soft soil during consolidation deformation. *Soils Found.* 61, 708–733. doi: 10.1016/j.sandf.2021.02.004